Cellular Retinaldehyde Binding Protein --Different Binding Modes and Micro-Solvation Patterns for High-Affinit....

Article *in* The Journal of Physical Chemistry B · August 2013

DOI: 10.1021/jp405410t · Source: PubMed

CITATIONS
5

READS
48

6 authors, including:

Rachel E. Helbling

13 PUBLICATIONS **21** CITATIONS

SEE PROFILE

Christin Bolze

Vifor Pharma

3 PUBLICATIONS **13** CITATIONS

SEE PROFILE

Marcin Golczak

Case Western Reserve University

94 PUBLICATIONS **3,527** CITATIONS

SEE PROFILE

Achim Stocker

Universität Bern

73 PUBLICATIONS **1,973** CITATIONS

SEE PROFILE

THE JOURNAL OF PHYSICAL CHEMISTRY B

Article

pubs.acs.org/JPCB

Cellular Retinaldehyde Binding Protein—Different Binding Modes and Micro-Solvation Patterns for High-Affinity 9-*cis*- and 11-*cis*-Retinal Substrates

Rachel E. Helbling,[†] Christin S. Bolze,[†,§] Marcin Golczak,[‡] Krzysztof Palczewski,[‡] Achim Stocker,*[,†] and Michele Cascella*[,†]

[†]Department of Chemistry and Biochemistry, University of Bern, Freiestrasse 3, 3012 Bern, Switzerland

[‡]Department of Pharmacology, School of Medicine, Case Western Reserve University, 2109 Adelbert Road, Cleveland, Ohio 44106-4965, United States

[§]Graduate School for Cellular and Biochemical Sciences, University of Bern, Switzerland

Supporting Information

ABSTRACT: We use molecular dynamics (MD) simulations to determine the binding properties of different retinoid species to cellular retinaldehyde binding protein (CRALBP). The complexes formed by 9-*cis*-retinal or 11-*cis*-retinal bound to both the native protein and the R234W mutant, associated to Bothnia-retina dystrophy, are investigated. The presented studies are also complemented by analysis of the binding structures of the CRALBP/9-*cis*-retinol and CRALBP/9,13-*dicis*-retinal complexes. We find that the poor X-ray scattering properties of the polyene tail of the ligand in all wild-type complexes can be attributed to a high mobility of this region, which does not localize in a single binding conformation even at very low temperatures. Our simulations report a clear difference in the residual solvation pattern in CRALBP complexes with either 9-*cis*- or 9,13-*dicis*-retinal. The reported structures indicate that the microsolvation properties of the ligand are the key structural element triggering the very recently discovered isomerase activity of this protein. The binding geometries obtained by MD simulations are validated by calculation of the respective optical spectra by the ZINDO/S semiempirical method, which can reproduce with good qualitative agreement the different red-shifts of the first absorption band of the different complexes.

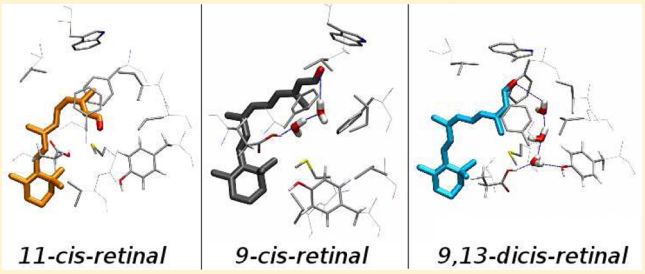

INTRODUCTION

Cellular retinaldehyde binding protein (CRALBP) is a 36 kDa soluble protein belonging to the Sec14-like protein family, whose members are crucial carriers of lipophilic molecules.[1,2] It was discovered in 1977 in bovine retina cytoplasm through its ability to bind exogenous radioactive 11-*cis*-retinoids.[3,4] CRALBP is located mainly in the retina pigment epithelium (RPE) as well as in the Müller glial cells of the retina.[5] Also, CRALBP has been found in the brain, giving rise to the hypothesis that it may be involved in other physiological functions than vision.[6,4] CRALBP is an essential transporter involved in the recycling of all-*trans*-retinal to 11-*cis*-retinal,[7] playing a hinge role in the retinoid visual cycle.[8,9] In RPE, CRALBP binds and transports 11-*cis*-retinol produced by RPE65 enzyme, and assists the oxidation of the retinoids to 11-*cis*-retinal by RDH5,[7,10,11] whereas, in the Müller glial cells, it is involved in the process of esterification of 11-*cis*-retinol.[12] CRALBP protects the retinoids from premature photoisomerization and from enzymatic back transformation into all-*trans* retinal[5,3,14] before they are transported from the RPE to the rod outer segment and to the photoreceptor.[8]

Substitution mutations of the CRALBP coding gene *RLBP1*[15,16] are known to cause severe genetic diseases, like Bothnia dystrophy.[17] The missense mutation associated with such a disease consists of the substitution of an arginine with a tryptophan residue at position 234, located in a basic patch at the protein surface putatively responsible for membrane binding (Figure 1).[5,18,19] Experimental data also show a smaller cavity for the ligand in the R234W mutant than in the wild-type, which leads to tighter binding of 11-*cis*-retinal. This may cause a less efficient release rate of 11-*cis*-retinal at the end of the transport cycle.[5,19]

Many efforts have been put in unveiling the exact function of CRALBP in the visual cycle, and in determining the molecular mechanisms at the origin of Bothnia dystrophy. In both cases, it is crucial to understand with high accuracy the binding properties at the molecular level of retinoids in CRALBP. Experimentally, crystal structures of the 11-*cis*-retinal bound to the wild-type protein (CRALBP/11-*cis*-retinal hereafter) and to R234W mutant (R324W/11-*cis*-retinal) have been solved.[5]

In recent times, new experimental data have been evidencing the ability of proteins belonging to the visual cycle to produce

Received: June 1, 2013
Revised: August 19, 2013
Published: August 21, 2013

dx.doi.org/10.1021/jp405410t | J. Phys. Chem. B 2013, 117, 10719−10729

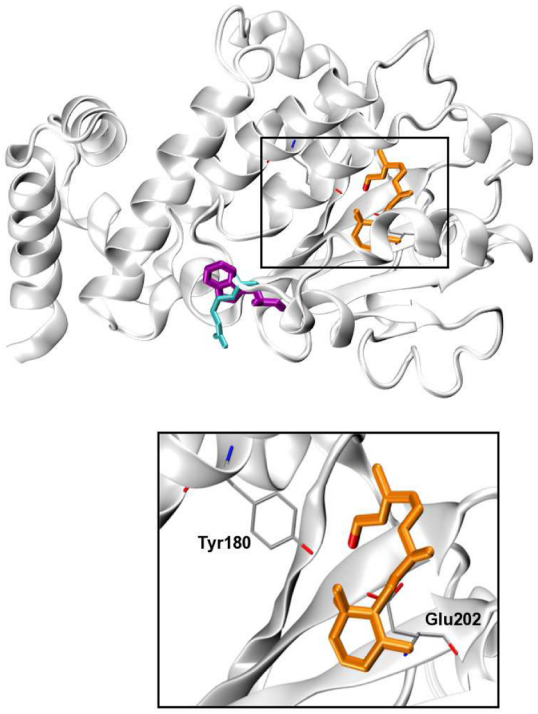

Figure 1. Three-dimensional structure of the CRALBP/11-*cis*-retinal complex.[5] The protein main-chain is drawn in white cartoon. 11-*cis*-retinal is drawn in orange licorice. R234W mutation is highlighted by cyan (CRALBP) and purple (R234W) licorices. Inset: binding cavity of CRALBP. Hydrophilic Tyr180 and Glu202 side-chains are represented by thin licorice.

and bind other *cis*-retinoids than the 11-*cis* isomers. For example, 9-*cis*-retinal forms isorhodopsin when bound to opsin,[20−22] a less efficient, albeit active, isoform of the photoreceptor. In addition, RDH5 presents some specificity toward 9-*cis*-retinal.[9] These facts may indicate the presence of pathways in the visual cycle able to consume residual *cis*-retinal isoforms different from the 11-*cis* one. In fact, *in vitro* data show that retinoids with different isomerization than all-*trans* or 11-*cis* are detected in negligible traces only.[13] This indicates that external physiological factors influence the activity of the proteins involved in the visual cycle, affecting the production of *cis*-isoforms of retinal other than 11-*cis*.

UV/Vis and ^{1}H NMR spectroscopic data demonstrated that CRALBP is able to bind 9-*cis*-retinoids.[4,11,13] Specifically, Crabb and co-workers determined an equilibrium dissociation constant for 9- and 11-*cis*-retinoids in the wild-type and in the R234W mutant.[11] 9-*cis*-retinal binds less tightly to CRALBP compared to the 11-*cis* isomer ($K_d \approx 53.3$ and 21.0 nM, respectively).[11] In the mutant protein, both ligands show instead a stronger affinity to the protein, with 9-*cis*-retinal remaining anyway less affine than 11-*cis*-retinal ($K_d \approx 24.3$ and 10.3 nM, respectively).[11]

In a very recent experiment by us, we demonstrated that CRALBP has isomerase activity in the dark, slowly but quantitatively converting 9-*cis*-retinal into 9,13-*dicis*-retinal.[23] In the same work, the structures of both CRALBP and its R234W mutant bound to 9-*cis*-retinal were also resolved by X-ray diffraction.[23] Consistently with the formerly deposited X-ray structures with 11-*cis*-retinal,[5] CRALBP/9-*cis*-retinal complexes produced systematically poorer data for the ligand, which could be only partially resolved. The only region of retinal that could be determined with comparable resolution to that of the protein was the bulky ionone ring. The R234W/9-*cis*-retinal crystals scattered well also in the polyene tail region of the ligand, again consistently with the R234W/11-*cis*-retinal structure. The reconstruction of the electronic density map for R234W/9-*cis*-retinal evidenced a distorted configuration of the ligand. Hybrid QM/MM calculations showed that the structure of 9-*cis*-retinal in R234W crystals suffered from radical damage, probably induced by the X-ray beam.[23] Nonetheless, the structural features emerged from the X-ray scattering allowed us to propose a mechanism for isomerization in the dark, involving catalytic attachment of a proton to the aldehyde group. Detection of strong nuclear-isotope effects in the kinetics of the reaction confirmed that proton transfer is the key step for the isomerization process.[23] The X-ray data of R234W/9-*cis*-retinal evidenced the presence of residual buried waters in the binding cavity. The isomerase function is not detected when 11-*cis* retinal binds to either CRALBP or the R234W mutant, suggesting that both the presence and the spatial organization of the water molecules in the pocket are crucial for the catalytic activity.[23] Given the poor quality of the X-ray scattering at the retinal region, it is not always possible to determine with sufficiently good accuracy the binding properties of retinoids in CRALBP, and more importantly the eventual presence and displacement of buried waters in the pocket.[5,23]

In this work, we use molecular dynamics (MD) simulations to provide a detailed molecular picture of the binding geometries of both 11-*cis* an 9-*cis*-retinal to wild-type and R234W CRALBP at physiological conditions. The structures of both 9,13-*dicis*-retinal and 9-*cis*-retinol in complex with CRALBP are also investigated (Figure 2). The computational

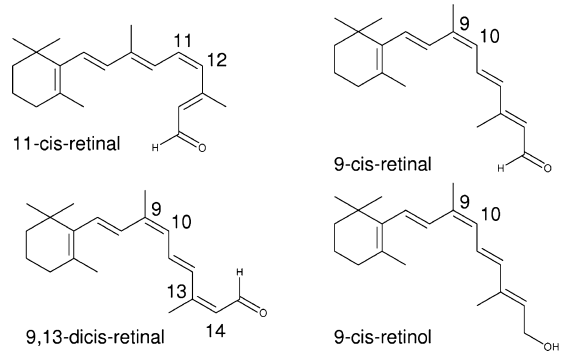

Figure 2. Chemical formulas of the studied retinoids.

models are validated by comparison with available experimental absorption spectra. Our findings allow for a clear understanding of the different binding properties of retinoids as well as their mobility and hydration in the binding pocket. The presented results provide a first structural explanation for the different activity of CRALBP as isomerase in the presence of different substrates or R234W mutation.

COMPUTATIONAL METHODS

System Setup. Molecular structures of both CRALBP and R234W mutant proteins bound to 11-*cis*-retinal were taken from the protein data bank (PDB entries: 3HY5 and 3HX3, respectively).[5] Titrable groups were protonated at standard positions at pH 7 except for residue Glu202, which was modeled as glutamic acid. This conserved residue is known to

be protonated in similar systems.[24] Also, the acid isoform is the most compatible with H-bond contacts evident from the X-ray structure,[5] and from an estimated pK_a value of 8.59 for the CRALBP/11-*cis*-retinal complex by PROPKA.[25−28]

The AMBER FF03[29] and the general Amber force field (GAFF)[30] were used to parametrize the protein and ligands, respectively. The RESP charge fitting procedure[31] was used to get the atomic charges of the retinals matching *ab initio* calculations at the HF/6-31G* level of theory. The same procedure was followed to set up two systems containing 9-*cis*-retinal bound to either CRALBP or the R234W mutant. The starting configuration of the CRALBP/9-*cis*-retinal complex was obtained from the 11-*cis*-retinal bound structure, aligning the ionone ring of the 9-*cis*-retinal to that of the 11-*cis*-retinal. For the R234W system, the starting structure was derived from the recently defined X-ray structure of the R234W/9-*cis*-retinal complex. As the scattering of 9-*cis*-retinal revealed damage by radical attachment, molecular replacement by intact 9-*cis*-retinal was performed to get the initial atomic coordinates. Nine/eight sodium cations were added to achieve charge neutrality in the CRALBP/mutant systems, respectively.

Additionally, two more models were built, investigating the wild-type protein in complex with 9,13-*dicis*-retinal as well as 9-*cis*-retinol ligands (Figure 2). The retinol species was again modeled by the GAFF force field, using the RESP procedure to determine point electrostatic charges. Initial docking of the ligands into the protein was achieved by aligning the ionone ring to the one present in the crystal structure or R234W. Three water molecules in the binding cavity, consistently with the 9-*cis*-retinal complexes, were added.

All systems were solvated by ∼23 000 TIP3P water molecules[32] for a total of ∼73 000 atoms, and contained periodic boxes of approximately 90 × 93 × 103 Å^3 initial dimensions.

Molecular Dynamics Simulations. The structures were originally relaxed by 300 cycles of steepest descent followed by 7200 cycles of conjugate gradients minimization procedures. A 100 ps run at constant temperature (310 K) and pressure (1 bar) keeping the protein immobile was performed to reach the correct density of liquid water. After that short simulation, the desired density of ∼1 g/mL was reached for the system, which was then minimized again with 300 cycles of steepest descent and 8500 cycles of conjugate gradients. Langevin dynamics for all non-hydrogen atoms was performed to equilibrate and keep the system at constant temperature (310 K) using a Langevin damping constant of 1 ps^{-1}. The modified Nosé−Hoover scheme[33−35] combined with Langevin pistons[36] was used to keep the system at constant pressure (1 bar), using a piston period of 200 fs and a piston decay of 50 fs. The particle-mesh Ewald (PME) method[37] was used to treat the long-range electrostatic interactions with a cutoff of 12 Å; the nonbonded list was updated every 10 steps. A time step of Δt = 2 fs was used. The SHAKE algorithm was used to freeze all bonds involving hydrogen atoms.[38] The relaxed structures of all the systems considered were used as starting points for 30 ns long MD simulations. All MD runs were performed using the NAMD 2.8 package.[39,40] The analysis of the trajectories was performed using different software tools available within the GROMACS 4.0.7 package.[41−44] The radial pair distribution functions were computed by the Amber tools package.[45]

Optical Spectra. Optical spectra of the retinals were computed using the ZINDO/S semiempirical method,[46] implemented in the Gaussian09 package.[47] For each system, the ligand, the buried waters, and all amino acids having at least one atom within a cutoff radius of 5 Å from any atom of the retinal were explicitly considered. The cut bonds were subsequently capped with hydrogen atoms. The same amino acids were considered in all calculations for all systems. The excitation bands were computed over a set of 30 independent structures taken from our MD trajectories with a time interval of 1 ns. Convolution of all single-point excitations obtained from the different snapshots was performed to obtain the global absorption band shape. Reference spectra of 11- and 9-*cis*-retinal in ethanol were also computed, using two independent 25 ns long simulations of the two retinal isomers in an ethanol box. The force-field parameters for the solvent were taken from ref 48.

RESULTS AND DISCUSSION

Binding Geometries of 11- and 9-*cis*-Retinal to CRALBP and R234W. Simulations of all CRALBP/retinal complexes show stable structures that deviate by less than 2 Å from the available crystal structure and their RMSDs do not increase after the first 15 ns of simulations. Average values for the RMSD are reported in Table S1 and Figure S1 (Supporting Information), with reference to the available X-ray data. The RMSD values of 11-*cis*-retinal with respect to the crystal structures are 2.89 and 2.71 Å, in the wild-type and mutant, respectively. The 9-*cis*-retinal instead displays RMSD values of 3.58 Å in the wild-type and 3.06 Å in R234W with respect to the analogous 11-*cis*-retinal crystal structures. Both retinal isomers show significantly high mobility in the binding cavity of the native protein. This is particularly true for the carbonyl region, where root-mean-square fluctuations (RMSFs) can be as high as 3.32 Å in the structures. On the contrary, the ionone ring shows in all cases a low mobility, with root-mean-square fluctuations around 1.0 Å. This is consistent with the fact that this portion of the molecule is the only one always detected by X-ray scattering. The R234W mutation leads to a significant decrease of the ligand mobility in the pocket in all of its regions. This is particularly true for the complex with 11-*cis*-retinal, where the RMSFs for the different atoms of the molecule are all ≈1.0 Å (Figure 3, Figures S2 and S3, Supporting Information). The mutation also decreases dramatically the volume of the cavity, from ≈5.41 × 10^4 Å^3 in the wild-type systems to ≈4.82 × 10^4 Å^3 in the mutant systems. However, the volumes of the retinoid isomers in the different protein remain quite similar, oscillating between 736 Å^3 in the wild-type systems and 739 Å^3 in the mutant systems. Nonetheless, the R234W mutation does not affect significantly the global fold of CRALBP, consistently with the X-ray data available.[5]

11-*cis*-Retinal Complexes. The ionone ring of retinal well sits in its pocket in both simulations of the 11-*cis*-retinal bound to CRALBP and the R234W mutant. No significant deviations from the crystallographic data available are reported for this region (Figure 4a). According to the deposited X-ray structure of the R234W/11-*cis*-retinal complex, the aldehyde terminus is an acceptor of hydrogen bonds from Glu202 and Tyr180. Our simulations indicate that both Glu202 and Tyr180 are only weakly bound to retinal. At room temperature, the two residues in contact with the aldehyde group are rather mobile, and the H-bonds between retinal and Glu202 or Tyr180 are only transiently formed during dynamics, as indicated by the statistical distribution of the distances between the oxygen atom of retinal and Glu202 and Tyr180 acid hydrogens (Figure 5). On the contrary, these contacts are better preserved in the

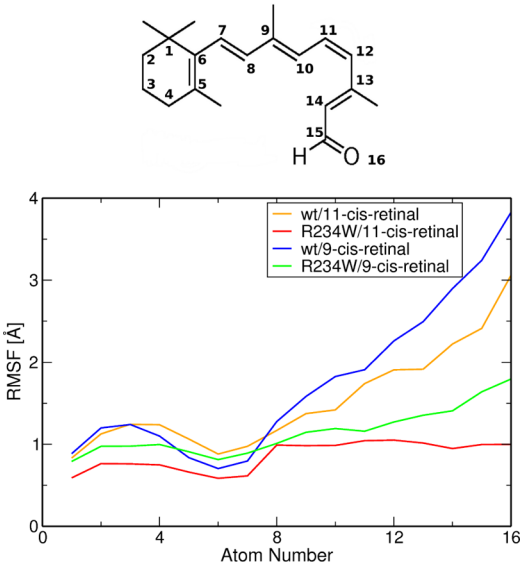

Figure 3. RMSF of the main-chain atoms of retinal. The graph reports computed data from MD simulations of the following complexes: CRALBP/11-*cis*-retinal (orange line), R234W/11-*cis*-retinal (red line), CRALBP/9-*cis*-retinal (blue line), and R234W/9-*cis*-retinal (green line).

mutant, where a single-peaked distribution is present for the H-bond formation between retinal and Glu202. In this system, the O−O distance with Tyr180 shows a bimodal distribution, where formation of a H-bond is detected for 36.8% of the simulated time only (Figure 5). In the conformation corresponding to the second distribution, the hydroxyl hydrogen is found oriented toward the carboxyl group of the Glu202 residue, with formation of H-bond characterized by an average oxygen−oxygen distance of 2.6 Å. This interaction stabilizes the orientation of the side-chain of Glu202 in the binding cavity.

In R234W, the statistical increase of H-bond interactions between the aldehyde group and the protein is induced by the reduced space in the binding pocket, which does not allow for the same mobility of the carbonyl and the side-chains of Glu202 and Tyr180 as in the wild-type. Quantitatively, the RMSF for the carbonyl group decreases from 2.56 Å in CRALBP to 0.98 Å in the R234W mutant (Figure 3). The RMSF of the side-chain of Glu202 also decreases from 0.95 to 0.67 Å.

Figure 5 reports the statistical distribution of these same contacts in CRALBP/11-*cis*-retinal at the temperature of the crystal (100 K). In this case, a single-peaked statistical distribution of the oxygen−oxygen distance between retinal and Glu202 is present; on the contrary, the contact with the tyrosine residue is formed for 64.3% of the simulated time only. In R234W/11-*cis*-retinal, instead, simulations at low temperature reveal a single-peaked distribution of distances between the carbonyl and Glu202 or Tyr180 (Figure 5). The presence of multiple binding modes for the aldehyde region of retinal already at low temperature can explain the poorer X-ray scattering properties of this portion of the molecule in CRALBP/11-*cis*-retinal crystals.[5] Conformational strain at the C_{12}−C_{13} bond is induced by the steric restraints imposed by the shape of the binding cavity. In our simulations, we report different isomerization from 11-*cis*,12-*s*-*trans*- to 11-*cis*,12-*s*-*cis*-retinal, in the two CRALBP and R234W proteins. In the first case, the 12-*s*-*cis* and 12-*s*-*trans* conformations occur in a ratio of 1:1 (Figure S4, Supporting Information), similar to the thermodynamic distribution in the free retinal originally reported in ref 49. In R234W, the 12-*s*-*cis* conformation is retained over the whole simulation (Figure S4, Supporting Information), also consistently with the X-ray data. The presence of multiple 12-*s* conformations in the complex with CRALBP can be another dynamical feature responsible for poor scattering of the polyene tail in X-ray measurements.

9-*cis*-Retinal Complexes. The crystallographic data for 9-*cis*-retinal complexes do not highlight retinal binding with good accuracy.[23] In fact, in CRALBP, the only region of retinal that can be detected is the ionone ring, while the R234W complex is reporting a damage in the ligand by H radical attachment at C_{12}.[23] In our simulations, 9-*cis*-retinal shows different binding structures than 11-*cis*-retinal in both CRALBP and the R234W mutant. The least structural differences are found for the ionone ring, which is localized in the same binding region of the 11-*cis*-retinal complexes. The molecular contacts between the ring and the protein are well conserved with respect to the crystallographic data in both CRALBP/9-*cis*-retinal and R234W complexes at low temperature. On the contrary, at room temperature, the wild-type complex shows a significant relaxation of the structure, leading to a RMSD of 1.90 Å for the ionone ring. The relaxation of the position of the ring is accompanied by a different orientation of the surrounding phenylalanine residues, namely, Phe161 and Phe173. Unlike the 11-*cis*-retinal systems, on which the residues are located on each side of the retinal and stabilize the methyl group of C_{13}, in CRALBP/9-*cis*-retinal, the ligand does not localize in proximity of these residues (Figure 4b,d).

Interestingly, in the more compressed binding cavity of R234W, the ionone ring of 9-*cis*-retinal keeps an orientation closer to that of 11-*cis*-retinal than in CRALBP at room temperature (average RMSD of the ionone rings between CRALBP/11-*cis*-retinal and R234W/9-*cis*-retinal: 1.22 Å). The position of the ring in our MD simulations is consistent with that evidenced in the X-ray structure of the R234W/9-*cis*-retinal complex, although there the detected ligand suffers from chemical modifications at C_{12}.[23]

In both the CRALBP and R234W, formation of hydrogen bonds between the aldehyde group and Glu202 or Tyr180 was not observed during the simulations. This is because of the different position of the *cis*-bond, which leads to a different curvature of the retinal in the pocket. As a result, the aldehyde group cannot remain in proximity of the only two hydrophilic residues present in the binding cavity without imposing a significant conformational strain to the whole molecule. The loss of contacts between the aldehyde and the side-chains of Glu202 or Tyr180 is consistent with what was observed in the R234W/9-*cis*-retinal crystals.[23] The carbonyl group localizes in a region defined by amino acids Ile163, Trp166, Phe173, and Leu215 in the wild-type. In the mutant, the contacts formed with the carbonyl oxygen atom include Phe161, Ile176, Leu177, as well as the aromatic ring of Tyr180 in the mutant. This last amino acid is, in fact, not able to form H-bond contacts with the aldehyde moiety; the average distance over simulation time between the two oxygen atoms is ≈7.2 Å in CRALBP and 5.2 Å in the mutant. Also, in this case, the conformational alternation between 9-*cis*,12-*s*-*trans*- and 9-*cis*,12-*s*-*cis*-retinal is different in CRALBP and R234W. In CRALBP, 9-*cis* retinal shows the tendency to stay in the 12-*s*-*trans* conformation, as shown by a *cis*/*trans* ratio of ∼1:3 (Figure S4, Supporting Information). In

dx.doi.org/10.1021/jp405410t | J. Phys. Chem. B 2013, 117, 10719−10729

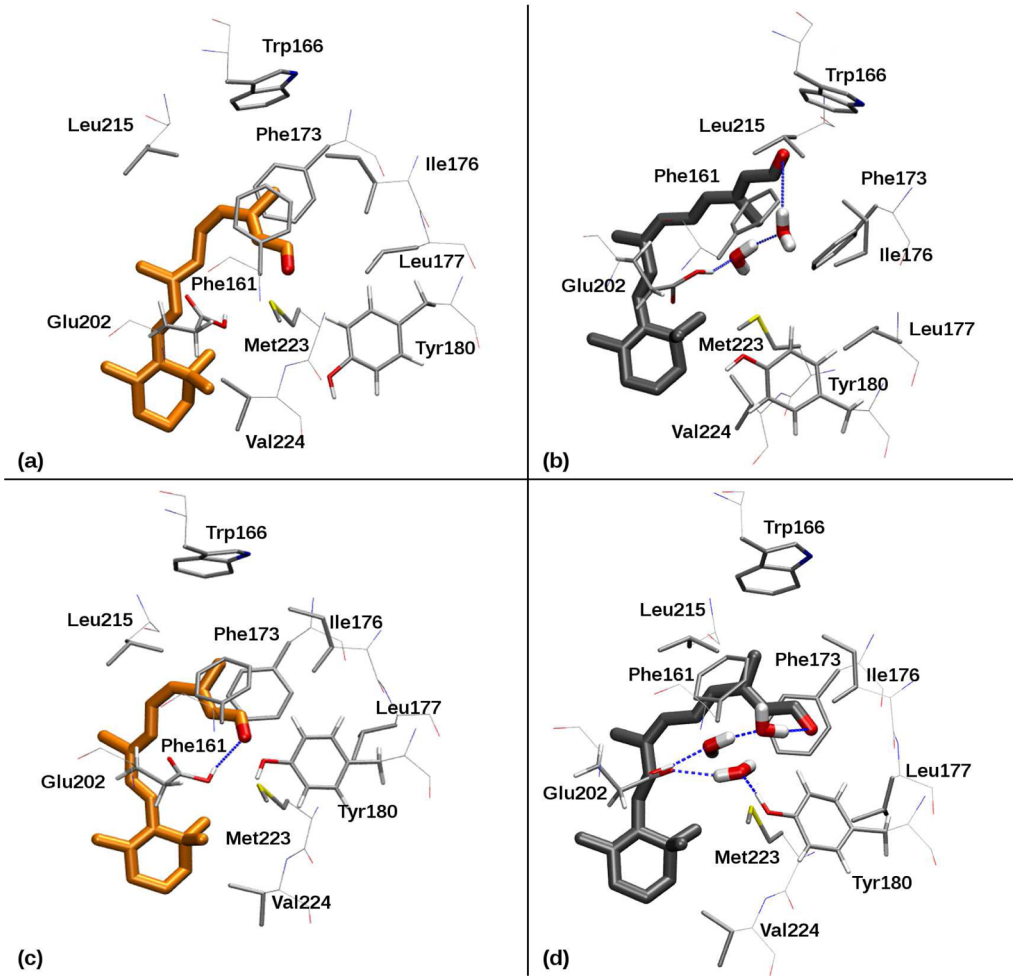

Figure 4. Average structures of the CRALBP/retinal complexes: 11-*cis*-retinal in complex with CRALBP (panel a) and R234W mutant (panel c); 9-*cis*-retinal in complex with CRALBP (panel b) and R234W mutant (panel d). Retinal molecules and buried waters are drawn in thick licorice, and neighboring groups are represented by thin licorice. H-bonds are highlighted by dashed blue lines. The rest of the protein and the surrounding solvent are not shown for the sake of clarity.

R234W, the conformation of the 12-*s* bond remains cis over the whole simulation time. Again, the 12-*s* conformation is consistent with the observed orientation of the aldehyde moiety in the X-ray image, even though, in this case, X-ray-induced radical damage of the substrate does not allow for a direct match with the simulated structure.

Hydration of the Pockets. The crystal structure of the R234W/9-*cis*-retinal complex evidences the presence of three buried waters in the binding cavity.[23] This constitutes a major difference with respect to structures of the complexes with 11-*cis*-retinal, where no crystallographic waters were detected.[5] The incomplete dehydration of the cavity can be attributed to the different binding geometry of 9-*cis*-retinal, in which both the aldehyde group of the ligand and the hydrophilic side-chains of Glu202 and Tyr180 would reside unscreened in a highly hydrophobic environment, unless residual water molecules are present. In our recent study,[23] we have postulated that the presence of buried waters in the pocket of CRALBP is crucial for its activity as isomerase enzyme, a previously unknown function of this protein. In fact, the isomerase activity is heavily affected by both the chemical nature of the ligand and the presence of the R234W mutation. Specifically, both CRALBP and R234W show no activity when bound to 11-*cis*-retinal. On the contrary, CRALBP irreversibly converts 9-*cis*-retinal to 9,13-*dicis*-retinal, while R234W shows a much faster kinetics for the same reaction, leading to thermodynamic equilibration between the two species.[23]

These marked differences in the activity can be putatively associated to a different hydration of the binding cavity in the different complexes. In all protein/retinal complexes, computation of surface accessible solvent area detected enough space in the binding cavity to accommodate, in principle, up to three waters. Therefore, we built different test systems where one, two, or three water molecules were introduced into the binding cavity at the beginning of the simulations. The initial positions of the water molecules were selected to maximize the agreement with computed solvent accessible spaces, and 9-*cis*-retinal bound systems, to allow the formation of H-bond with Glu202, the only strong water−protein contact present in the X-ray structure of the R234W/9-*cis*-retinal complex. All MD simulations of complexes involving 11-*cis*-retinal systematically led to complete dehydration of the binding pocket. Specifically, all water molecules initially placed in the cavity were expelled into the bulk solvent within the first 2 and 8 ns of MD simulations for the CRALBP and R234W systems, respectively. In fact, in these complexes, the carbonyl head of the retinal and the side-chains of Glu202 and Tyr180, the only hydrophilic groups present in the cavity, reside in close proximity.

dx.doi.org/10.1021/jp405410t | J. Phys. Chem. B 2013, 117, 10719−10729

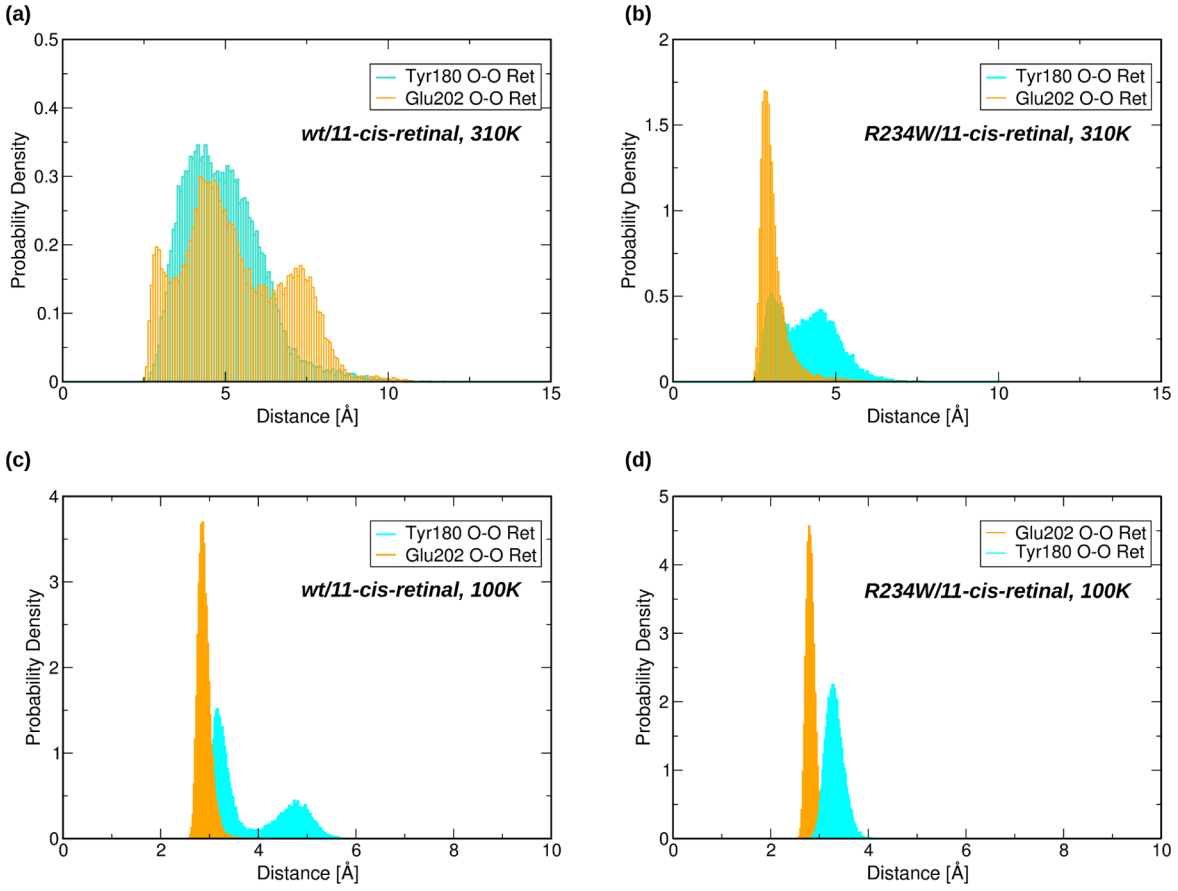

Figure 5. Statistical distributions of the distances between the oxygen atoms of 11-*cis*-retinal and those of Glu202 and Tyr180. Panels a and b report distances in the complex with CRALBP and R234W at physiological temperature. Panels c and d report the respective statistical distributions at 100 K.

Therefore, they are not able to efficiently bind to the water. As a result, the water molecules in the binding pocket remain significantly under-coordinated, maintaining a high mobility, and they leave the pocket as soon as any thermal fluctuation of the protein structure allows for unbinding. As the cavity of the mutant is more rigid than that of the wild-type, it is reasonable that the characteristic times for water expulsion from the cavity are systematically shorter for CRALBP than for R234W.

In MD simulations of the CRALBP/9-*cis*-retinal complex, we observe the stable presence of two water molecules in the binding cavity. In this complex, the aldehyde group is connected to Glu202 by a H-bond network formed by two bridging water molecules. The average oxygen−oxygen distances for the different H-bonds present in the cavity are $(Glu)O-O(H_2O)$, 2.9 Å; $(H_2O)O-O(H_2O)$, 2.7 Å; $(H_2O)O-O(retinal)$, 2.9 Å (Figure 4b). The proximity of the aromatic ring of Trp166 to the carbonyl suggests additional π-stacking interaction stabilizing the retinal end. Different from the 11-*cis*-retinal complexes, the presence of residual water molecules in the pocket is crucial to stabilize the hydrophilic moieties in the cavity, which, in this case, are not in direct contact with each other. The number of water molecules detected in the 9-*cis*-retinal complexes is different from that found in the crystallographic structure of the complex with R234W. In fact, we repeated different MD runs where three water molecules were originally placed inside the cavity, using three different initial positions for the waters, and repeating the runs imposing different random starting velocities for the water molecules. In all of these simulations, we reported extrusion of one water molecule from the binding cavity already during the initial minimization procedure.

MD simulations of the R234W/9-*cis*-retinal complex confirm the presence of three water molecules in the binding pocket, consistently with the X-ray diffraction data.[23] The slightly different binding geometry of the retinal from that in CRALBP reflects subtle differences in the hydration pattern. Similarly to CRALBP, two buried waters build a H-bond network connecting the side-chain of Glu202 with retinal. The third water is located in a niche on the side of the first two water molecules, and acts as a H-bond donor for both Glu202 and Tyr180 (Figure 4d). This water can also accept a hydrogen bond from the other water molecule in contact with Glu202. Compared to the X-ray structure of R234W/9-*cis*-retinal, where damage by H· attachment at C_{12} of retinal occurs, the average RMSD of retinal non-hydrogen atoms in our relaxed structure from MD is 2.12 Å. The position of Glu202 is instead well preserved as indicated by the RMSD of 0.94 Å for the non-hydrogen atoms of this residue.

The different binding mode of the intact 9-*cis*-retinal than that of the species detected by X-ray scattering is also characterized by a slightly different organization of the water molecules around the aldehyde group. While the two water molecules bridging Glu202 to the carbonyl oxygen are conserved in both structures, the third water is, in our simulations, topologically distant from the first two, and it is in contact with the carbonyl group. In the crystal structure, it is

dx.doi.org/10.1021/jp405410t | J. Phys. Chem. B 2013, 117, 10719−10729

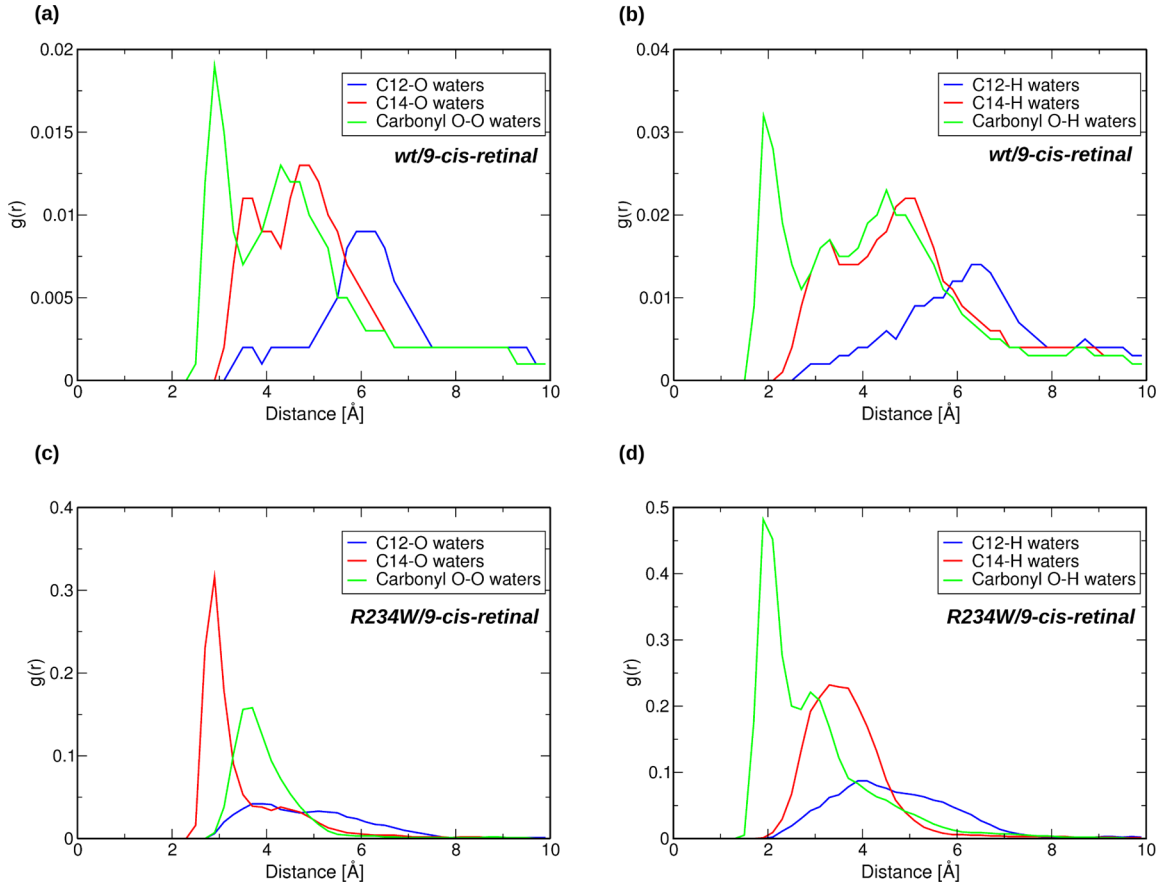

Figure 6. Radial distribution functions between selected 9-*cis*-retinal atoms and surrounding waters in the binding cavity. Upper panels refer to the CRALBP/9-*cis*-retinal complex, while lower panels report data for R234W/9-*cis*-retinal. The distribution for water oxygens (panels a and c) and hydrogens (panels b and d) are shown. Radial distribution functions are computed from atoms C_{12} (blue lines), C_{14} (red lines), and oxygen (green line) of retinal.

directly H-bonded to the first two water molecules, and it does not directly interact with the aldehyde oxygen. The different displacement of this water is not surprising, as the damaged retinal shows a significant twist of the carbonyl of roughly 155° from the nondamaged structure. We also note that the space occupied by one of the water molecules in our MD simulations is partially occupied, in the crystal structure, by the methyl group attached to the C_{13} atom. This also contributes to the different organization of the waters between the simulation of the undamaged 9-*cis*-retinal and the X-ray data.

Figure 6 reports the radial distribution functions (RDFs) of the waters in the pocket with respect to atoms C_{12}, C_{14}, and O of retinal for both CRALBP/9-*cis*-retinal and R234W/9-*cis*-retinal complexes.

In the CRALBP/9-*cis*-retinal system, the first peak of the different RDFs with water oxygen atoms are at ∼3 Å from O, at ∼3.7 Å from C_{14}, and at ∼6.3 Å from C_{12} (Figure 6). The water distributions highlight that, contrary to the aldehyde tail, the central segment of the retinal molecule is only very weakly hydrated. These results are consistent with the experimental evidence of *trans*−*cis* isomerization occurring at the C_{13}−C_{14} bond, which can take place after protonation of the aldehyde moiety and consequent change in bond-order at C_{13}−C_{14}. The corresponding RDFs of the water hydrogen atoms show a first intense peak at ∼2.0 Å from O, corresponding to hydrogen bond formation. Nonetheless, a first peak at ∼3.2 Å appears in the RDF from C_{14}. This feature points at the presence of a non-negligible number of configurations where water protons may be activated for direct transfer to the C_{14} atom.

Therefore, our simulations point at the enol form as the most probable to be produced upon proton transfer to the retinal; nonetheless, our data cannot exclude the possible formation of keto-adducts in the pocket, even though experiments in deuterated water tend to exclude it.[23] In this respect, future investigations at the quantum-mechanical level to accurately determine the molecular details of the isomerization process are envisaged.

The RDFs for the R234W/9-*cis*-retinal system present a different distribution pattern, in particular for the C_{12}-water oxygen atoms. There, the peak of the distribution shifts from ∼6.3 to ∼4.0 Å (Figure 6). In particular, the integration of the radial distribution of the water hydrogen atoms from the C_{12} position up to a distance of 4 Å passes from 0 to 0.429. The statistical abundance of hydrogen atoms in close proximity to C_{12} justifies the behavior of this atom as a Lewis base, and the consequent protonation at this site seen in the damaged X-ray structure of the R234W/9-*cis*-retinal complex.

Optical Spectra. The various CRALBP/retinal complexes show different absorption spectra. In particular, all complexes are red-shifted with respect to the absorption band of retinals in ethanol solution. Nonetheless, the complexes with 11-*cis*-retinal show stronger red-shift with respect to those with 9-*cis*-retinal. We validated the computed structures of the CRALBP/retinal complexes by checking that they reproduce the same main

features in the absorption band in the visible. Excited state spectra calculations have been computed at the semiempirical ZINDO/S method,[46,47] which had been previously successfully used to evaluate relative shifts in the absorption spectra of other protein−retinoid complexes.[24,50,51] Table 1 reports the calculated spectra, in comparison to the experiment.[11,52,53] The computed results are in very good quantitative agreement with the experiment, thus confirming the reliability of the MD structures. Nevertheless, given the approximations used in the calculations, the results obtained should be interpreted at a qualitative more than a quantitative level.

Table 1. Comparison between Calculated and Measured Absorption Spectra of Retinal Absorbance in Ethanol Solution and in Different Complexes with CRALBP[a]

	calculated (nm)	measured (nm)
11-*cis*-retinal in ethanol	372.56 ± 15.77	380.0
9-*cis*-retinal in ethanol	374.35 ± 14.20	373.0
CRALBP/11-*cis*-retinal	435.90 ± 11.21	425.0
R234W/11-*cis*-retinal	435.44 ± 14.06	425.3
CRALBP/9-*cis*-retinal	407.17 ± 10.46	400
R234W/9-*cis*-retinal	416.05 ± 10.93	408.3

[a]Experimental data are from refs 52 for the compounds in ethanol, 53 for the wild-type complexes, and 11 for the R234W complexes, respectively.

In particular, our calculations show that the additional red-shift of the 11-*cis*-retinal/CRALBP complexes has to be attributed to the different topological position of the retinal in the binding cavity. In fact, in the 11-*cis*-retinal complexes, fluctuations of the geometry allow for the activation of electronic transitions characterized by charge-transfer states involving the extended π-system of retinal, and the π-systems of Tyr180, Glu202, and, transiently, Phe161 (Figure 7). These transitions cannot be active in the 9-*cis*-systems, where Tyr180 and Glu202 remain constantly far from retinal.

Binding of 9-*cis*-Retinol and 9−13-*dicis*-Retinal to CRALBP. In order to build up first hypotheses on any eventual implication into the visual cycle of the newly found isomerase function of CRALBP,[23] it is crucial to get structural insights about other CRALBP/retinoid complexes involved in this process. Within the present work, we have built models of both CRALBP/9-*cis*-retinol and CRALBP/9,13-*dicis*-retinal complexes. These two systems represent the following limit situations: (i) CRALBP/9-*cis*-retinol—this is the first complex between CRALBP and a 9-*cis*-retinoid isoform formed during the visual cycle; (ii) CRALBP/9,13-*dicis*-retinal—this is the

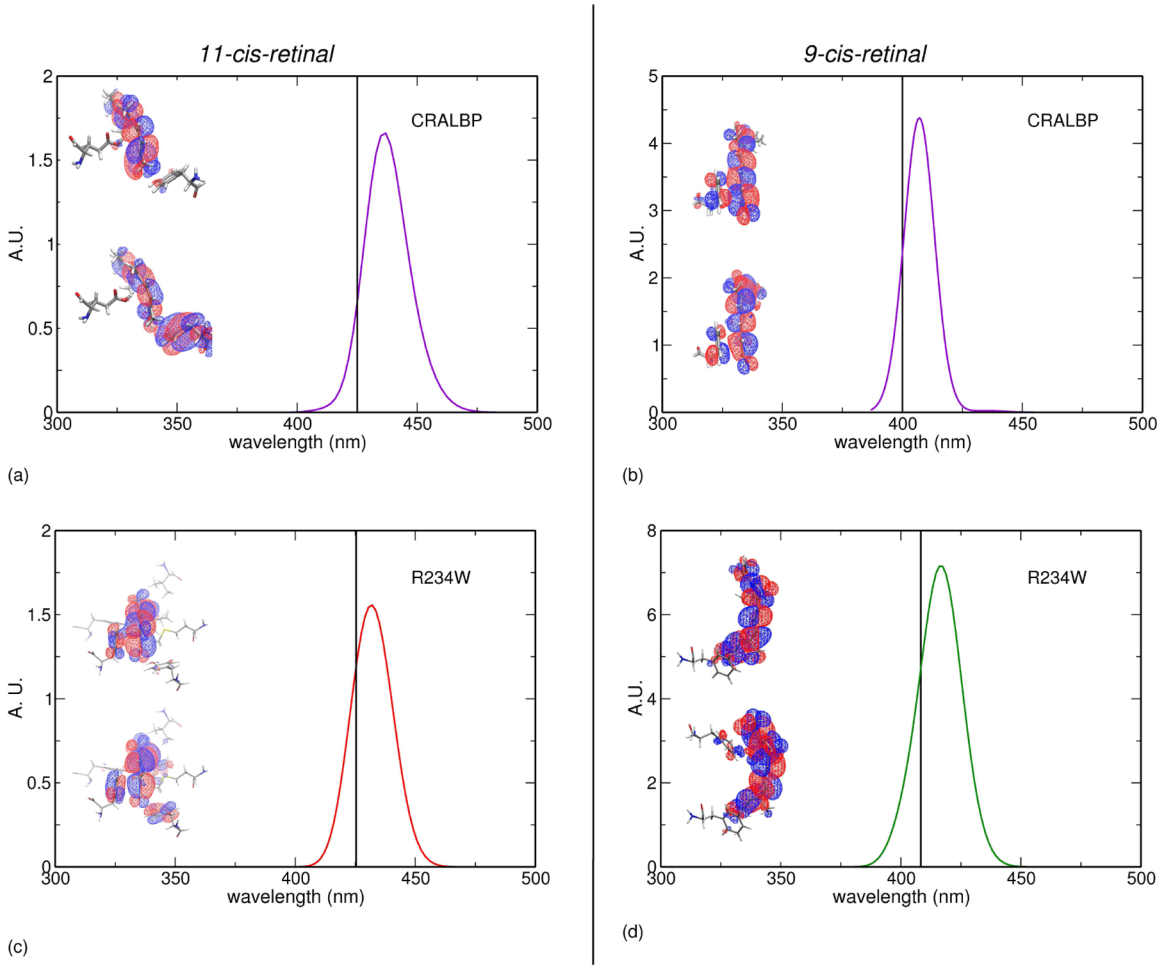

Figure 7. Calculated optical spectra for different protein/retinal complexes: CRALBP/11-*cis*-retinal (upper left), CRALB/9-*cis*-retinal (upper right), R234W/11-*cis*-retinal (bottom left), and R234W/9-*cis*-retinal (bottom right) complexes. The black straight line reports the experimental maximum peak of absorption, taken form ref 53 for the wild-type and ref 11 for the R234W mutant, respectively. The insets show the character of the HOMO−LUMO transitions primarily involved in photoabsorbtion.

dx.doi.org/10.1021/jp405410t | J. Phys. Chem. B 2013, 117, 10719−10729

complex detected in our recent experiment after 9-*cis*-retinal isomerization.

9-*cis*-retinol presents a different binding in CRALBP compared to the retinal ligands, as suggested by the high RMSD of 5.40 Å of the crystal structure of CRALBP/11-*cis*-retinal (Table S1, Supporting Information). Interestingly, the protein does not show a significant distortion, compared to the other systems. The ionone ring is more mobile than in retinal complexes (RMSF = 1.97 Å), and a notable difference between both retinoids can be attributed to a distortion of the $C_1-C_6-C_7-C_8$ dihedral angle of ~20°, compared with the X-ray of CRALBP/11-*cis*-retinal. The alcohol group in CRALBP/9-*cis*-retinol is in close proximity with water molecules and Phe161, and does not show significant mobility during the simulation (RMSF of $C_{14}-C_{15}-O$ atoms: 1.17 Å), different from the carbonyl moiety of retinal. The hydration pattern is slightly different from the CRALBP/9-*cis*-retinal complex. In fact, in this case, three water molecules hydrate the retinol group. The H-bond network between the retinol and the Glu202/Tyr180 region is instead similar to those previously described, with the water molecules connecting the alcohol functional group to the side-chain of Glu202 (Figure 8b).

The ionone ring in the CRALBP/9,13-*dicis*-retinal complex is displaced with respect to the position of CRALBP/9-*cis*-retinal. In particular, the ionone ring of 9,13-*dicis*-retinal localizes in closer proximity to the hydrophobic residues Phe240 and Phe247, while in the CRALBP/9-*cis*-retinal complex contacts are formed with Tyr251 and Phe204 aromatic groups.

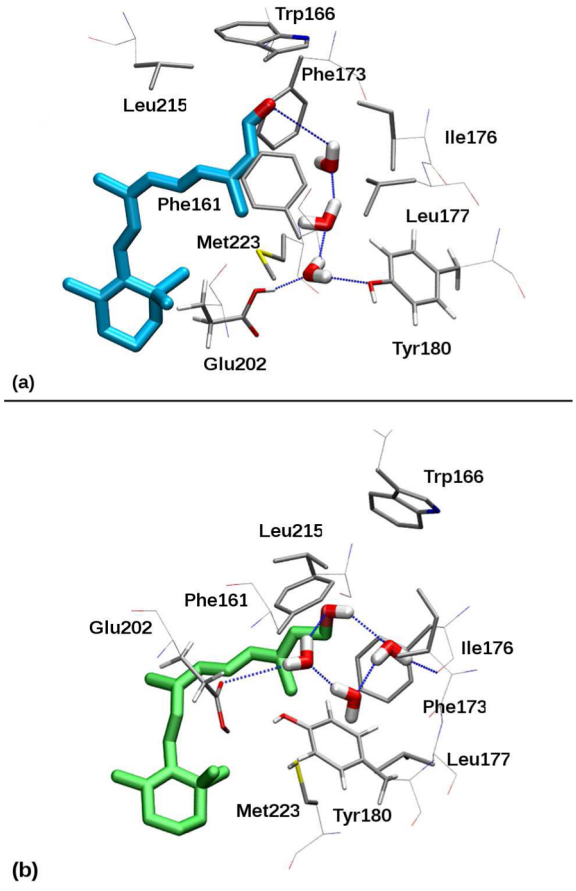

Figure 8. Average structures of CRALBP/9,13-*dicis*-retinal (panel a) and CRALBP/9-*cis*-retinol complexes (panel b). Retinal molecules and buried waters are drawn in thick licorice, and neighboring groups are represented by thin licorice. H-bonds are highlighted by dashed blue lines. The rest of the protein and the surrounding solvent are not shown for the sake of clarity.

The carbonyl oxygen is located in a space formed by Phe161, Trp166, Phe173, and Ile176 (Figure 8a). In particular, the carbonyl oxygen of the 9,13-*dicis*-retinal is in close proximity to Trp166, as indicated by an average O−N distance of 3.88 Å. Interestingly, the same feature is found in the 9-*cis*-retinal in CRALBP. The carbonyl oxygen is pointing toward the indol ring in both cases, leading to the assumption that this contact plays a non-negligible role in the stability of the carbonyl group in 9-*cis*-isomers. In our simulations, both two or three water molecules can be accommodated in the binding pocket. When three waters are bound, one of them bridges Glu202 and Tyr180; in any case, the typical H-bond network linking Glu202 to the carbonyl group is respected, as depicted in Figure 8. Nevertheless, in this case, the glutamic acid can act as a hydrogen bond acceptor, a feature significantly different from all the other systems. The hydration structure with three water molecules is instead particularly similar to that of the X-ray image of the CRALBP/9-*cis*-retinal complex. That structure is, in fact, characterized by a partial 11-*cis* character, induced by the deformation at C_{12} from X-ray induced H radical attachment. This points to the possibility that this particular H-bond pattern is characteristic of *dicis*-retinoids bound to CRALBP. CRALBP/9,13-*dicis*-retinal is formed upon isomerization in CRALBP/9-*cis*-retinal. Therefore, the same number of waters could be, in principle, expected in the pocket. In fact, it is possible that a third water could enter in the pocket upon relaxation of the system after the isomerization of the substrate. In particular, the two complexes differ for a different displacement of the ionone ring. This part of the molecule is in contact with the lid-helix,[5] and in all CRALBP complexes, local fluctuations of the structure in that region of the protein show transient opening of the pocket to the solvent.

The increased number of water molecules in the pocket can be functional to the isomerase activity, decreasing the efficiency of the catalytic proton transfer from Glu202 to retinal, thus significantly slowing down reverse isomerization to 9-*cis*-retinal. In fact, during MD, solvation structures characterized by two water molecules bridging the Tyr and the Glu residues have been observed. Substantial differences in the residual hydration of the hydrophobic binding pocket with chemically very similarly bound substrates has been previously reported for α-tocopherol transfer protein, a homologous species of CRALBP.[54]

CONCLUDING REMARKS

We determined the binding properties of both 11-*cis*- and 9-*cis*-retinal to CRALBP and its R234W mutant by molecular dynamics simulations. The calculated structures were validated by calculation of the absorption spectra, which well reproduced the different red-shifts of the various complexes. In our studies, we found that the ligand in the CRALBP/11-*cis*-retinal complex respects the global orientation found in the X-ray structure of the R234W/11-*cis*-retinal one. In particular, the aldehyde group sits in proximity of the side-chains of Tyr180 and Glu202. Different from the complex with R234W, in CRALP, the carbonyl does not make strong H-bond contacts to these groups, also showing large fluctuations from its average position. The weak contacts with the protein, and the relatively large mobility, are at the base of the poor scattering properties of this region of the retinal molecule during X-ray experiment.

dx.doi.org/10.1021/jp405410t | J. Phys. Chem. B 2013, 117, 10719−10729

9-*cis* complexes show strong differences from those with 11-*cis*-retinal. In fact, the different position of the *cis* bond does not allow the aldehyde to lay in proximity of the two Tyr180 and Glu202. Rather, the carbonyl remains in a hydrophobic environment close to Trp166. In these complexes, the binding cavity is not completely dehydrated. A minimal number of buried waters ensures hydration of the hydrophilic residues, and of the carbonyl. The presence of water molecules in the binding pocket is associated with the isomerase activity recently detected. Our computations reveal the presence of a hydrogen-bond network connecting Glu202 to the carbonyl group. This network can constitute an efficient proton shuttle system able to transiently protonate the aldehyde region, and thus catalyze the $C_{13}-C_{14}$ isomerization. In R234W, water molecules reside in close proximity of C_{12}, thus enhancing the possibility of proton transfer at this site. This confirms the original hypothesis of a coupled electron−proton transfer, triggered by X-ray scattering, at the base of the structural damage observed in the crystallographic image of the R234W/9-*cis*-retinal complex.

The presented results show a first step toward the understanding of the molecular details by which CRALBP exerts alternate binding modes for 11-*cis*- and 9-*cis*-retinoids. The differences in the microsolvation of the binding regions of the various complexes, identified by our MD simulations, are associated to the experimentally reported modulation of the isomerase activity. The presented models give access to future research activities aiming at understanding the functional role of CRALBP in both the visual cycle and other non-image-forming processes, as well as in replacement therapies by 11-*cis*-retinal surrogates.

■ ASSOCIATED CONTENT

Supporting Information

RMSD values and graphs for the studied systems, statistical distributions of the 12-*s* dihedral angle, conformational mobility of the retinoids in the studied systems, parameter sets for retinal and retinol, and full author list for refs 11, 23, 29, 45, and 47. This material is available free of charge via the Internet at http://pubs.acs.org.

■ AUTHOR INFORMATION

Corresponding Author

*E-mail: michele.cascella@iac.unibe.ch (M.C.); achim.stocker@ibc.unibe.ch (A.S.). Phone: +41 (0)31 631 4256. Fax: +41 (0)31 631 3994.

Notes

The authors declare no competing financial interest.

■ ACKNOWLEDGMENTS

The presented research was funded by the Swiss National Foundation (Grant No. PP00P2_139195 for M.C. and 31003A_130497 for A.S.). K.P. is John Hord Professor of Pharmacology. The authors wish to thank Prof. Ursula Röthlisberger for enlightening discussion.

■ REFERENCES

(1) Panagabko, C.; Morley, S.; Hernandez, M.; Cassolato, P.; Gordon, H.; Parsons, R.; Manor, D.; Atkinson, J. Ligand Specificity in the CRAL-TRIO Protein Family. *Biochemistry* **2003**, *42*, 6467−6474.

(2) von Lintig, J.; Kiser, P. D.; Golczak, M.; Palczewski, K. The Biochemical and Structural Basis for Trans-to-Cis Isomerization of Retinoids in the Chemistry of Vision. *Trends Biochem. Sci.* **2010**, *35*, 400−410.

(3) Saari, J. C.; Bunt, A. H.; Futterman, S.; Berman, E. R. Localization of Cellular Retinol-Binding Protein in Bovine Retina and Retinal Pigment Epithelium, with a Consideration of the Pigment Epithelium Isolation Technique. *Invest. Ophtalmol. Vis. Sci.* **1977**, *16*, 797−806.

(4) Crabb, J. W.; Carlson, A.; Chen, Y.; Goldflam, S.; Intres, R.; West, K. A.; Hulmes, J.; Kapron, J.; Luck, L.; Horwitz, J.; Bok, D. Structural and Functional Characterization of Recombinant Human Cellular Retinaldehyde-Binding Protein. *Protein Sci.* **1998**, *7*, 746−757. 10th Symposium of the Protein-Society, San Jose, CA, Aug 3−7, 1996.

(5) He, X.; Lobsiger, J.; Stocker, A. Bothnia Dystrophy is Caused by Domino-Like Rearrangements in Cellular Retinaldehyde-Binding Protein Mutant R234W. *Proc. Natl. Acad. Sci. U.S.A.* **2009**, *106*, 18545−18550.

(6) Saari, J. C.; Huang, J.; Possin, D. E.; Fariss, R. N.; Leonard, J.; Garwin, G. G.; Crabb, J. W.; Milam, A. H. Cellular Retinaldehyde-Binding Protein is Expressed by Oligodendrocytes in Optic Nerve and Brain. *Glia* **1997**, *21*, 259−268.

(7) Saari, J. C.; Nawrot, M.; Kennedy, B. N.; Garwin, G. G.; Hurley, J. B.; Huang, J.; Possin, D. E.; Crabb, J. W. Visual Cycle Impairment in Cellular Retinaldehyde Binding Protein (CRALBP) Knockout Mice Results in Delayed Dark Adaptation. *Neuron* **2001**, *29*, 739−748.

(8) Palczewski, K. Chemistry and Biology of Vision. *J. Biol. Chem.* **2012**, *287*, 1612−1619.

(9) Kiser, P. D.; Golczak, M.; Maeda, A.; Palczewski, K. Key Enzymes of the Retinoid (Visual) Cycle in Vertebrate Retina. *Biochim. Biophys. Acta* **2012**, *1821*, 137−151.

(10) Saari, J. C.; Bredberg, D. L.; Noy, N. Control of Substrate Flow at a Branch in the Visual Vycle. *Biochemistry* **1994**, *33*, 3106−3112.

(11) Golovleva, I.; Bhattacharya, S.; Wu, Z.; Shaw, N.; Yang, Y.; Andrabi, K.; West, K. A.; Burstedt, M. S. I.; Forsman, K.; Holmgren, G.; et al. Disease-Causing Mutations in the Cellular Retinaldehyde Binding Protein Tighten and Abolish Ligand Interactions. *J. Biol. Chem.* **2003**, *278*, 12397−12402.

(12) Muniz, A.; Villazana-Espinoza, E. T.; Thackeray, B.; Tsin, A. T. C. 11-cis-Acyl-CoA:Retinol O-Acyltransferase Activity in the Primary Culture of Chicken Muller Cells. *Biochemistry* **2006**, *45*, 12265−12273.

(13) Saari, J. C.; Bredberg, D. L. Photochemistry and Stereoselectivity of Cellular Retinaldehyde-Binding Protein from Bovine Retina. *J. Biol. Chem.* **1987**, *262*, 7618−7622.

(14) McBee, J. K.; Van Hooser, J. P.; Jang, G.-F.; Palczewski, K. Isomerization of 11-Cis-Retinoids to All-Trans-Retinoids in Vitro and in Vivo. *J. Biol. Chem.* **2001**, *276*, 48483−48493.

(15) Burstedt, M. S. I.; Sandgren, O.; Holmgren, G.; Forsman-Semb, K. Bothnia Dystrophy Caused by Mutations in the Cellular Retinaldehyde-Binding Protein Gene (RLBP1) on Chromosome 15q26. *Invest. Ophtalmol. Vis. Sci.* **1999**, *40*, 995−1000.

(16) Lamb, T. D.; Pugh, E. N. Dark Adaptation and the Retinoid Cycle of Vision. *Prog. Retinal Eye Res.* **2004**, *23*, 307−380.

(17) Burstedt, M. S. I.; Forsman-Semb, K.; Golovleva, I.; Janunger, T.; Wachtmeister, L.; Sandgren, O. Ocular Phenotype of Bothnia Dystrophy, an Autosomal Recessive Retinitis Pigmentosa Associated with an R234W Mutation in the RLBP1 Gene. *Arch. Ophtalmol.* **2001**, *119*, 260−267.

(18) Liu, T. Y.; Jenwitheesuk, E.; Teller, D. C.; Samudrala, R. Structural Insights into the Cellular Retinaldehyde-Binding Protein (CRALBP). *Proteins* **2005**, *61*, 412−422.

(19) Wu, Z.; Hasan, A.; Liu, T.; Teller, D. C.; Crabb, J. W. Identification of CRALBP Ligand Interactions by Photoaffinity Labeling, Hydrogen/Deuterium Exchange, and Structural Modeling. *J. Biol. Chem.* **2004**, *279*, 27357−27364.

(20) Crouch, R.; Purvin, V.; Ladd, C. Isorhodopsin II: Artificial Photosensitive Pigment Formed from 9,13-Dicis Retinal. *Proc. Natl. Acad. Sci. U.S.A.* **1975**, *72*, 1538−1542.

(21) Crouch, R.; Pepperberg, D. R. Sensitizing Activity of 9,13-dicis Retinal in Bleached Photoreceptors of the Skate. *Invest. Ophtalmol. Vis. Sci.* **1978**, *17*, 1024−1029.

(22) Fan, J.; Rohrer, B.; Moiseyev, G.; Ma, J.-X.; Crouch, R. K. Isorhodopsin Rather than Rhodopsin Mediates Rod Function in RPE65 Knock-out Mice. *Proc. Natl. Acad. Sci. U.S.A.* **2003**, *100*, 13662−13667.
(23) Bolze, C. S.; Helbling, R. E.; Owen, R. L.; Pearson, A. R.; Pompidor, G.; Dworkowski, F.; Fuchs, M.; Furrer, J.; Golczak, M.; Palczewski, K.; et al. Manuscript Submitted for Publication.
(24) Röhrig, U. F.; Guidoni, L.; Rothlisberger, U. Early Steps of the Intramolecular Signal Transduction in Rhodopsin Explored by Molecular Dynamics Simulations. *Biochemistry* **2002**, *41*, 10799−10809.
(25) Li, H.; Robertson, A. D.; Jensen, J. H. Very Fast Empirical Prediction and Rationalization of Protein pKa Values. *Proteins* **2005**, *61*, 704−721.
(26) Bas, D. C.; Rogers, D. M.; Jensen, J. H. Very Fast Prediction and Rationalization of pKa Values for Protein−Ligand Complexes. *Proteins* **2008**, *73*, 765−783.
(27) Olsson, M. H. M.; Søndergaard, C. R.; Rostkowski, M.; Jensen, J. H. PROPKA3: Consistent Treatment of Internal and Surface Residues in Empirical pKa Predictions. *J. Chem. Theory Comput.* **2011**, *7*, 525−537.
(28) Søndergaard, C. R.; Olsson, M. H. M.; Rostkowski, M.; Jensen, J. H. Improved Treatment of Ligands and Coupling Effects in Empirical Calculation and Rationalization of pKa Values. *J. Chem. Theory Comput.* **2011**, *7*, 2284−2295.
(29) Duan, Y.; Wu, C.; Chowdhury, S.; Lee, M. C.; Xiong, G. M.; Zhang, W.; Yang, R.; Cieplak, P.; Luo, R.; Lee, T.; Caldwell, J. W.; et al. A Point-Charge Force Field for Molecular Mechanics Simulations of Proteins Based on Condensed-Phase Quantum Mechanical Calculations. *J. Comput. Chem.* **2003**, *24*, 1999−2012.
(30) Wang, J. M.; Wolf, R. M.; Caldwell, J. W.; Kollman, P. A.; Case, D. A. Development and Testing of a General Amber Force Field. *J. Comput. Chem.* **2004**, *25*, 1157−1174.
(31) Cornell, W. D.; Cieplak, P.; Bayly, C. I.; Gould, I. R.; Merz, K. M.; Ferguson, D. M.; Spellmeyer, D. C.; Fox, T.; et al. A 2nd Generation Force-Field for the Simulation of Proteins, Nucleic-Acids, and Organic-Molecules. *J. Am. Chem. Soc.* **1995**, *117*, 5179−5197.
(32) Jorgensen, W. L.; Chandrasekhar, J.; Madura, J. D.; Impey, R. W.; Klein, M. L. Comparison of Simple Potential Functions for Simulating Liquid Water. *J. Chem. Phys.* **1983**, *79*, 926−935.
(33) Nose, S. A Molecular-Dynamics Method for Simulations in the Canonical Ensemble. *Mol. Phys.* **1984**, *52*, 255−268.
(34) Hoover, W. G. Canonical Dynamics - Equilibrium Phase-Space Distributions. *Phys. Rev. A* **1985**, *31*, 1695−1697.
(35) Martyna, G. J.; Klein, M. L.; Tuckerman, M. Nose-Hoover Chains - The Canonical Ensemble via Continuous Dynamics. *J. Chem. Phys.* **1992**, *97*, 2635−2643.
(36) Feller, S. E.; Zhang, Y. H.; Pastor, R. W.; Brooks, B. R. Constant-Pressure Molecular-Dynamics Simulation - The Langevin Piston Method. *J. Chem. Phys.* **1995**, *103*, 4613−4621.
(37) Essman, U.; Perera, L.; Berkowitz, M. L.; Darden, T.; Lee, H.; Pedersen, L. G. A Smooth Particle Mesh Ewald Method. *J. Chem. Phys.* **1995**, *103*, 8577−8593.
(38) Ryckaert, J.-P.; Ciccotti, G.; Berendsen, H. J. C. Numerical Integration of the Cartesian Equations of Motion of a System with Constraints: Molecular Dynamics of n-Alkanes. *J. Comput. Phys.* **1977**, *23*, 327−341.
(39) Phillips, J. C.; Braun, R.; Wang, W.; Gumbart, J.; Tajkhorshid, E.; Villa, E.; Chipot, C.; Skeel, R. D.; Kalé, L.; Schulten, K. Scalable Molecular Dynamics with NAMD. *J. Comput. Chem.* **2005**, *26*, 1781−1802.
(40) University of Illinois at Urbana-Champaign, NIH Center for Macromolecular Modeling and Bioinformatics, http://www.ks.uiuc.edu/Research/namd/.
(41) Van der Spoel, D.; Lindahl, E.; Hess, B.; Groenhof, G.; Mark, A. E.; Berendsen, H. J. C. GROMACS: Fast, Flexible, and Free. *J. Comput. Chem.* **2005**, *26*, 1701−1718.
(42) Berendsen, H. J. C.; van der Spoel, D.; van Drunen, R. GROMACS - A Message-Passing Parallel Molecular-Dynamics Implementation. *Comput. Phys. Commun.* **1995**, *91*, 43−56.
(43) Lindahl, E.; Hess, B.; van der Spoel, D. GROMACS 3.0: a Package for Molecular Simulation and Trajectory Analysis. *J. Mol. Model.* **2001**, *7*, 306−317.
(44) Hess, B.; Kutzner, C.; van der Spoel, D.; Lindahl, E. GROMACS 4: Algorithms for Highly Efficient, Load-Balanced, and Scalable Molecular Simulation. *J. Chem. Theory Comput.* **2008**, *4*, 435−447.
(45) Case, D. A.; Darden, T. A.; Cheatham, T. E., III; Simmerling, C. L.; Wang, J.; Duke, R. E.; Luo, R.; Walker, R. C.; Zhang, W.; Merz, K. M.; et al. *AMBER 11*; University of California: San Francisco, CA, 2010.
(46) Ridley, J.; Zerner, M. Intermediate Neglect of Differential Overlap Technique for Spectroscopy - Pyrrole and Azines. *Theor. Chim. Acta* **1973**, *32*, 111−134.
(47) Frisch, M. J.; Trucks, G. W.; Schlegel, H. B.; Scuseria, G. E.; Robb, M. A.; Cheeseman, J. R.; Scalmani, G.; Barone, V.; Mennucci, B.; Petersson, G. A.; et al. *Gaussian 09*, revision B.01; Gaussian, Inc.: Wallingford, CT, 2009.
(48) Dupradeau, F.-Y.; Cézard, C.; Lelong, R.; Stanislawiak, É.; Pêcher, J.; Delepine, J. C.; Cieplak, P. R.E.DD.B.: A Database for RESP and ESP Atomic Charges, and Force Field Libraries. *Nucleic Acids Res.* **2008**, *36*, D360−D367.
(49) Rowan, R.; Warshel, A.; Sykes, B. D.; Karplus, M. Conformation of Retinal Isomers. *Biochemistry* **1974**, *13*, 970−981.
(50) Alberto Montero-Cabrera, L.; Roehrig, U. F.; Padron-Garcia, J. A.; Crespo-Otero, R.; Montero-Alejo, A. L.; Garcia de la Vega, J. M.; Chergui, M.; Rothlisberger, U. CNDOL: A Fast and Reliable Method for the Calculation of Electronic Properties of Very Large Systems. Applications to Retinal Binding Pocket in Rhodopsin and Gas Phase Porphine. *J. Chem. Phys.* **2007**, *127*, 145102.
(51) Valsson, O.; Campomanes, P.; Tavernelli, I.; Rothlisberger, U.; Filippi, C. Rhodopsin Absorption from First Principles: Bypassing Common Pitfalls. *J. Chem. Theory Comput.* **2013**, *9*, 2441−2454.
(52) Gundersen, T. E.; Blomhoff, R. Qualitative and Quantitative Liquid Chromatographic Determination of Natural Retinoids in Biological Samples. *J. Chromatogr., A* **2001**, *935*, 13−43.
(53) Crabb, J. W.; Nie, Z.; Chen, Y.; Hulmes, J. D.; West, K. A.; Kapron, J. T.; Ruuska, S. E.; Noy, N.; Saari, J. C. Cellular Retinaldehyde-Binding Protein Ligand Interactions. *J. Biol. Chem.* **1998**, *273*, 20712−20720.
(54) Helbling, R. E.; Aeschimann, W.; Simona, F.; Stocker, A.; Cascella, M. Engineering Tocopherol Selectivity in α-TTP − a Combined in Vitro/in Silico Study. *PLoS One* **2012**, *7*, e49195.